Field-induced structures and transitions in chiral antiferroelectric liquid crystals

P. V. Dolganov and V. M. Zhilin
Institute of Solid State Physics, Russian Academy of Sciences, Chernogolovka 142432, Moscow Region, Russia
(Received 19 September 2007; published 18 March 2008)

The transformation of a chiral antiferroelectric liquid crystal in an electric field was calculated. Minimization of the free energy was performed with respect to both the phase and the modulus of the two-component order parameter. Competition between the electric field, which favors a planar structure, and chirality and the anticlinic ordering leads to frustration and sequential formation of a distorted helix, a soliton state, transition to an unwound distorted antiferroelectric, and finally the planar synclinic state. In the soliton and distorted antiferroelectric states an anomalous electroclinic effect (the decrease of the tilt angle and layer polarization) was found. The antiferroelectric soliton can be removed by a large electric field only via the transition to the synclinic state.

DOI: 10.1103/PhysRevE.77.031703 PACS number(s): 61.30.Cz, 64.70.M−

I. INTRODUCTION

The electric-field-induced transitions from antiferroelectric to ferroelectric structure in liquid crystals are of substantial interest for use in a new generation of display devices and from the viewpoint of fundamental physics. In these materials the molecules are arranged into smectic layers with their long molecular axes tilted with respect to the layer normal (Fig. 1). In the antiferroelectric smectic-C_A^* (SmC_A^*) phase, the long molecular axes tilt in nearly opposite directions in adjacent layers, and these anticlinic molecular pairs form a twisted structure in which the tilt plane rotates from layer to layer. Field-induced helix unwinding in simpler structures, namely, cholesteric (N^*) and ferroelectric (SmC^*) phases, is a well-known phenomenon. It was studied earlier by many experimental and theoretical research groups [1–10] starting from the classic works of de Gennes [1] and Meyer [2]. In theoretical studies, a continuous theory could be used since the orientation of molecules changes only slightly along the helix both in N^* (twisted nematic) and in SmC^* (synclinic ordering).

Field-induced phenomena in antiferroelectric liquid crystals are more complicated and essentially different from those of N^* and SmC^*, due to the overlapping of several processes, particularly the unwinding of the long-pitch helix and the transition from anticlinic to synclinic ordering. In antiferroelectric structures, frustration arises from the competition of the electric field, which favors a planar structure, with both chirality, which favors a twist, and anticlinic ordering. Pioneering theoretical studies by Taylor *et al.* were made for the anticlinic structure without the helix and for a fixed value of the molecular tilt angle [11–13]. Even in such nontwisted structures, complex behavior in an electric field was found [12,13]. The first calculations of twisted antiferroelectric showed drastic changes of the antiferroelectric helix in an electric field [14]. Moreover, the antiferroelectric-ferroelectric transition occurs at a larger electric field than the unwinding field of the ferroelectric helix. It is thus necessary to consider the change of the tilt angle of molecules, θ, in an electric field. In our paper, the antiferroelectric-ferroelectric transition is studied using a discrete phenomenological model based on the Landau theory of phase transitions [15–26]. The discrete model was first proposed by Sun, Orihara, and Ishibashi [15]. They assumed that the phase transition into the tilted smectic phase (SmC) should take place in noninteracting smectic layers. The nonchiral and chiral interactions between layers led to formation of polar phases. The discrete model [15] also explained the reversing of the helical sense at the SmC_A^*-SmC^* phase transition. Čepič and Žekš [16] extended this model for description of the short-pitch incommensurate SmC_α^* phase. Later, the discrete model was used to describe the structure and the sequence of the fundamental and intermediate phases [17–26]. In this simulation, we used the discrete model to calculate different antiferroelectric states in an electric field, accounting for the chirality and the change of the tilt angle of molecules, θ (electroclinic effect).

II. MODEL

The polar smectic structure is modeled as a stack of layers with a two-component (2D) vector order parameter ξ_i, where

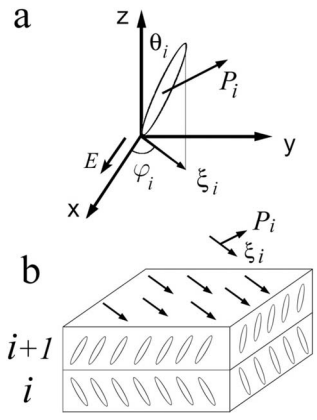

FIG. 1. Schematic representation of the model geometry. Orientation of molecules (a) and layer structure (b) in the antiferroelectric phase. θ_i and φ_i are the polar and azimuthal angles. The two-component vector ξ_i is the order parameter. Each molecular layer bears the electric polarization $\mathbf{P}_i$ perpendicular to ξ_i. The helical axis is along the z direction. The electric field $\mathbf{E}$ is applied along the x axis.

i stands for the ith layer (Fig. 1). The modulus of ξ_i is the projection of the long molecular axis onto the layer plane and characterizes the polar tilt angle θ_i (Fig. 1). The phase of the order parameter, φ_i, characterizes the azimuthal orientation of the tilt plane in the ith layer. The system is uniform in the xy plane. The free energy can be written as an expansion over the structural (ξ) and polar ($\mathbf{P}$) order parameters. Minimization of the free energy with respect to the polarization gives a relation between ξ and $\mathbf{P}$ [20,21]. The final energy depends only on ξ with renormalized coefficients of expansion. The base expansion of the free energy density for coupled smectic layers reads

$$F = \sum_i \left(\frac{1}{2}\alpha(T - T^*)\xi_i^2 + \frac{1}{4}b\xi_i^4 + \frac{1}{2}a_1\xi_i\xi_{i+1} \right). \quad (1)$$

The first two terms are the Landau expansion describing the transition to the untilted smectic-A (SmA) phase [27]. The last term describes the interactions between adjacent layers. The parameter a_1 corresponds to both van der Waals interaction and the interaction between the polarizations in adjacent layers, the piroelectric and flexoelectric coupling [20,21]. A positive coefficient a_1 favors anticlinic ordering, while a negative a_1 promotes synclinic ordering. Our model of the antiferroelectric structure in the electric field includes also three additional terms. First, the chiral interaction leading to formation of a helix is presented in the free energy by the Lifshits term, which is taken in the form

$$F_{\mathrm{ch}} = \sum_i f(\xi_i \times \xi_{i+1})_z. \quad (2)$$

Next, to get the first-order antiferroelectric-ferroelectric transition, one has to introduce a term representing an energetic barrier between synclinic and anticlinic structures. The simplest barrier term can be written as

$$F_b = \sum_i a_2(\xi_i \times \xi_{i+1})^2. \quad (3)$$

The energy barrier between the synclinic and anticlinic states (fourth-order term) was introduced already in the continuous model of the antiferroelectric phase by Orihara and Ishibashi [28]. They obtained several types of phase sequence depending on the coefficient of the fourth-order term. F_b describes the quadrupolar interaction between nearest layers [19]. The barrier plays an important role in the discrete model. In particular, the existence of the energy barrier explains reentrant ferroelectricity [19] and distorted clock structures [20]. A strong quadrupolar interaction at low temperature leads to a first-order transition to the ferroelectric state in the electric field [13,29]. Finally, the external electric field E, which is applied along the x-axis direction, couples with the transverse polarization of smectic layers and hence with the order parameter. The electric polarization P_i within a layer is perpendicular to ξ_i (Fig. 1). The corresponding term may be written in the form

$$F_e = \sum_i Ec|\xi_i|\sin\varphi_i, \quad (4)$$

where the value of the layer polarization is $P_i = c|\xi_i|$. In zero electric field, the model with $a_1 > 0$, $f \neq 0$ leads to nearly anticlinic ordering of adjacent layers and a helix along the z axis. Equilibrium structures were calculated by numerical minimization of the free energy over both the phase φ_i and the modulus θ_i of the order parameter ξ_i for each i. In the simulations we used model parameters leading to unperturbed pitch P_0 from 13 to 40 layer spacings d. The thickness of the sample was from $250d$ to $500d$. For such thicknesses the boundary distortion does not affect the bulk behavior inside the system. The method of numerical minimization of the free energy was described earlier [23]. Further, for the sake of simplicity we set $b=1$ and measure α in units of 1/K. The value of α in the calculations was chosen so that the order parameter modulus θ was about 20° at $T_C - T = 10$ K, where T_C is the temperature of the transition to the untilted SmA state. This value corresponds to the typical observed tilt angle. The azimuthal orientation of the tilt plane φ_i is taken in the range from $-\pi$ to π. The electric field is given in nondimensional units Ec/a_1.

III. FIELD-INDUCED STRUCTURES AND TRANSITIONS IN THE ELECTRIC FIELD

First we describe the behavior of the helical antiferroelectric structure in an electric field qualitatively. The orientations of the vectors ξ_i in different structures are shown in Fig. 2. In zero field a uniform antiferroelectric helix exists [Fig. 2(a)]. The anticlinic helix can be conceived as follows [Fig. 2(a)]: a pair of molecules (or ξ_i in our model) in adjacent layers with nearly anticlinic ordering rotates by a relatively small angle $\Delta\varphi = 2\pi d/P_0$ and translates along z over two layer spacings d. In electric field the helix becomes distorted [Figs. 2(b) and 2(f)] and the period of the structure increases. Unlike ferroelectric SmC^*, where in an electric field there is only one transition to an unwound ferroelectric, in antiferroelectrics there are several regimes of structural transformations and two lines of transitions. The first one is the winding-unwinding transition at the critical threshold E_h [Figs. 2(b) and 2(c)]. Above the unwinding field [Fig. 2(c)] the system becomes spatially uniform. In this structure ξ_i orient only in two planes [Fig. 2(c)]. The angle between the corresponding tilt planes $\Delta\varphi = \varphi_1 - \varphi_2$ decreases with increasing field [Fig. 2(d)], and at a second critical field E_s this leads finally to the transition to a homogeneous synclinic state in which all ξ_i orient in the same direction perpendicular to the electric field [Fig. 2(e)].

A. Distorted winding antiferroelectric phase

Let us now focus on a comprehensive description of the winding-unwinding transition at which the pitch diverges. We will show how the system responds to frustration in the antiferroelectric material. For the description of structural transformations we will use the following parameters: the winding angle $\varphi_i^W = (\varphi_i - \varphi_{i+2})/2$, which characterizes the helicity, and the distortion angle $\varphi_i^D = (\varphi_i - \varphi_{i+1})$, which charac-

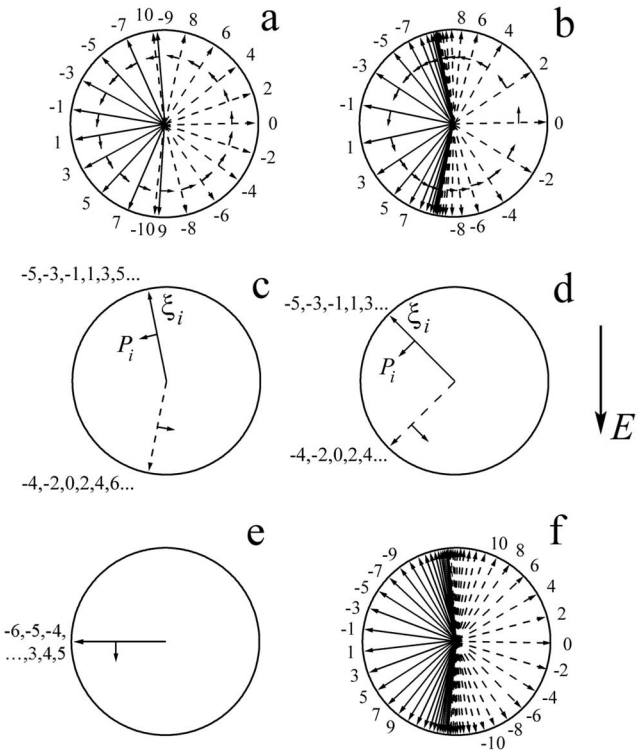

FIG. 2. Antiferroelectric material in electric field. Long solid and dotted arrows show the orientation of the vector order parameter ξ_i in odd and even layers. Short arrows show the layer polarization $\mathbf{P}_i$ [see (c)]. Calculations were made using Eqs. (1), (2), and (4). Numbers indicate the smectic layer. (a) Initial winding state with a regular helix ($E=0$). (b) Distorted winding state ($E \lesssim E_h$). The ξ_i between walls group near two tilt planes. (c) Distorted antiferroelectric ($E \gtrsim E_h$) with a spatially uniform structure. The ξ_i orient in two tilt planes. (d) Distorted antiferroelectric for larger field ($E \approx 0.7E_s$). (e) Ferroelectric synclinic state ($E > E_s$). All ξ_i orient perpendicular to the electric field $\mathbf{E}$. Model parameters are $\alpha = 0.01$, $f/a_1 = 8.5 \times 10^{-2}$, and $a_1 = 5 \times 10^{-2}$. The helical pitch without the electric field is about 18.7 layers. (f) Distorted winding state ($E \lesssim E_h$). Model parameters are $\alpha = 0.01$, $f/a_1 = 4.2 \times 10^{-2}$, $a_1 = 5 \times 10^{-2}$, and $T_C - T = 5$ K. The helical pitch in absence of the electric field is about 37.5 layers.

terizes the similarity of the structure to either synclinic ($\varphi_i^D = 0$) or anticlinic ($|\varphi_i^D| = \pi$) ordering. In zero field a uniform antiferroelectric helix with $\varphi_i^D = \text{const}$ and $\varphi_i^W = \text{const}$ is formed [Figs. 2(a) and 3(a)]. In the electric field φ_i^W and φ_i^D change along the structure and the helix becomes distorted. The structure can be divided into two types of region. I n a simple way it can be described by domains with small winding angle φ_i^W separated by domain walls with φ_i^W larger than in zero field [Fig. 3(b)]. Formation of the walls occurs as follows. The electrostatic energy of anticlinic pairs $F_{ei} = -(\mathbf{P}_i + \mathbf{P}_{i+1})\mathbf{E}$. In small field $F_{ei} = 2Ec|\xi_i|\sin(\varphi_i + \varphi_{i+1})/2 \cos \varphi_i^D/2$ changes sign from layer to layer because of the $\sin(\varphi_i + \varphi_{i+1})/2$ factor. In Fig. 3 on the left side of the wall $F_{ei} < 0$ for i even. On the right side of the wall $F_{ei} < 0$ for i odd. We will discuss in detail the left side of the wall. In order to decrease the electrostatic energy, the ξ_i rotate so that φ_i^D decreases for i even and increases for i odd. This change

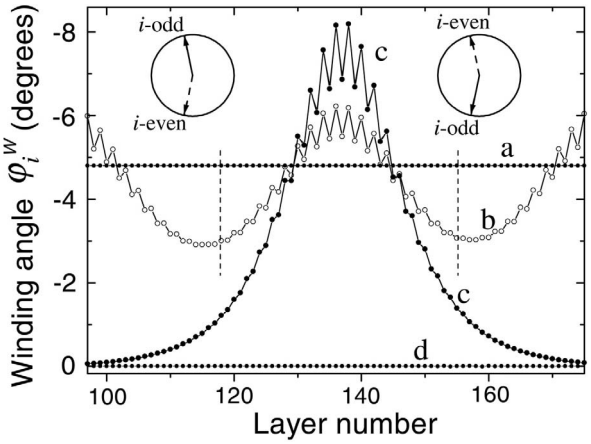

FIG. 3. Transformation of the winding angle $\varphi_i^W = (\varphi_i - \varphi_{i+2})/2$ in electric field. φ_i^W characterizes the helicity in the system. (a) Antiferroelectric state, $E=0$, $\varphi_i^W = \text{const}$. The dotted lines show the value of the undistorted pitch. (b) A domain wall in an electric field ($Ec/a_1 = 2.8 \times 10^{-2}$). (c) Antiferroelectric soliton in high field E close to but smaller than E_h ($Ec/a_1 = 4.1 \times 10^{-2}$). The insets show schematically the orientation of ξ_i in odd and even layers on the two sides of the soliton. Far from the soliton, the ξ_i orient nearly parallel or antiparallel to the electric field $\mathbf{E}$. (d) Planar synclinic state, $\varphi_i^W = 0$ ($Ec/a_1 = 0.54$). Model parameters are $\alpha = 0.01$, $f/a_1 = 4.2 \times 10^{-2}$, $a_1 = 5 \times 10^{-2}$, and $T_C - T = 5$ K.

is more pronounced in the region where the ξ_i are nearly parallel or antiparallel to $\mathbf{E}$ (anticlinic pairs are nearly symmetric with respect to the axis perpendicular to $\mathbf{E}$). When the modulus of the distortion angle $|\varphi_i^D|$ with i odd reaches a value larger than π, F_{ei} also become negative for i odd. As E increases, the number of such pairs increases. From the region where the initial orientations of ξ_i are nearly parallel or antiparallel to $\mathbf{E}$, a "switching wave" (changing the sign of $\cos \varphi_i^D/2$ with i odd) moves in two opposite directions increasing the pitch and forming walls. Between walls the ξ_i are grouped near two angles [Fig. 2(b)]. In relatively high fields ($E \sim E_h$) an antiferroelectric soliton is formed [Fig. 3(c)].

B. Soliton state

We describe now the special features of the antiferroelectric soliton. In the soliton regime the structure consists of nearly uniform regions and a single wall (soliton). The total change of the winding angle φ_i^W in the soliton is π. In the soliton the center angles φ_i^W are larger for layers with $F_{ei} > 0$, i.e., for i even in Fig. 2(b). Outside the soliton φ_i^W is nearly zero [Fig. 3(c)]. The structural peculiarities of the antiferroelectric soliton and the coupling of the modulus and the phase of the order parameter are demonstrated by the "phase portrait" of the soliton, i.e., the relation between θ_i and φ_i (Fig. 4). The points represent the values of the 2D order parameter. The numbers of layers in this figure are counted from the layer in the central part of the soliton ($i = 0$, Fig. 4). Lines link points in adjacent layers. The circles describe ξ_i on the left side of the soliton. The squares stand

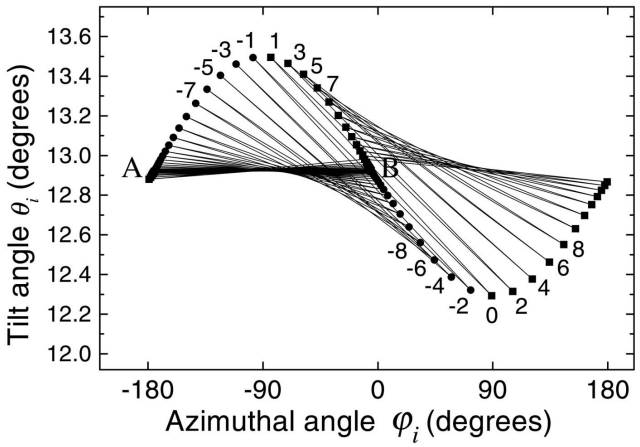

FIG. 4. Phase portrait of an antiferroelectric soliton. The dependence of the modulus of the order parameter (tilt angle θ_i) on the phase of the order parameter (azimuthal orientation of molecules φ_i) is shown by points. Lines link points in adjacent layers. Numbers of layers in this figure are counted from ξ_0 in the central part of the soliton. Layers in the central part of the soliton are depicted by the points in the upper and lower parts of the phase portrait. Circles (squares) describe ξ_i on the left (right) side of the soliton center. Model parameters are $\alpha=0.01$, $f/a_1=4.2\times10^{-2}$, $a_1=5\times10^{-2}$, $Ec/a_1=4.1\times10^{-2}$, and $T_C-T=5$ K.

for ξ_i on the right of the soliton center. In the soliton the tilt angle θ_i alternately increases and decreases from layer to layer. This effect is most pronounced in the soliton center, where the vectors $\mathbf{P}_i$ are nearly parallel or antiparallel to the electric field. The tilt angle is larger in layers in which $\mathbf{P}_i$ and $\mathbf{E}$ are directed nearly parallel and smaller in neighboring layers with opposite directions of $\mathbf{P}_i$ and $\mathbf{E}$ (the top and bottom parts of the phase portrait, respectively).

The points located near A and B in Fig. 4 correspond to layers far from the soliton. These regions are characterized by a nearly fixed modulus of the order parameter (nearly horizontal lines in the figure). Its value is somewhat smaller than that in the zero-field state. The orientation of ξ_i on two sides of the soliton is shown by the insets in Fig. 3. The modulus of the distortion angle $|\varphi_i^D|$ is nearly constant but the orientations of ξ_i are correspondingly reversed for i odd and i even on the two sides of the soliton. The latter means in particular that domains on the left and right sides of the soliton cannot be connected other than by a switching wave, which flips the orientations of ξ_i on one side of the soliton. By contrast, in the ferroelectric soliton these domains can adjoin each other without formation of a defect. The antiferroelectric soliton cannot be removed in a simple way. The soliton can exist as a metastable state at $E>E_h$. However, even in the metastable soliton state, heating of a part of the sample with a soliton to the SmA phase (setting $\xi_i=0$) and subsequent cooling lead the system back to the soliton state. Similar manipulations with a ferroelectric soliton lead to its disappearance and formation of the planar synclinic state. The antiferroelectric soliton can be removed in a large electric field only via the transition to the synclinic state. In the ferroelectric soliton state, most molecules outside the soliton orient so that layer polarizations are nearly parallel to the electric field. By contrast, in the antiferroelectric soliton state most molecules orient so that layer polarizations are nearly perpendicular to the electric field. This orientation is conserved after the transition to the unwound state (see below).

C. Untwisted distorted antiferroelectric

The unwinding regime is ended at the critical threshold E_h by the transition to the untwisted ($\varphi_i^W=0$) distorted antiferroelectric state without solitons [Fig. 2(c)]. At this transition the modulus of the distortion angle $|\varphi_i^D|$ remains nearly the same for the molecules outside the soliton. The value of the distortion angle $|\varphi_i^D|$ at the unwinding transition depends on the pitch of the unperturbed helix without field. $|\varphi_i^D|$ increases with increasing pitch. Note that in the untwisted state the molecules in even (and correspondingly odd) layers tilt in one plane in the whole sample [compare Fig. 2(c) and the insets in Fig. 3]. In an untwisted antiferroelectric, the ξ_i are oriented approximately along the applied field. This structure and the orientations of ξ_i are consistent with the experimental observations [30–32]. The deviation from anticlinic order ($|\varphi_i^D|\neq\pi$) leads to a macroscopic polarizarion $\mathbf{P}_r$ [33] in the distorted antiferroelectric state. In higher fields $|\varphi_i^D|$ decreases [Fig. 2(d)], $\mathbf{P}_r$ increases and finally, at the critical field E_s, the planar synclinic state ($\varphi_i^D=0$) is formed [Figs. 2(e) and 3(d)]. It is well known [27] that the applied electric field interacts with the liquid crystal also through the dielectric permittivity. The corresponding term in the smectic liquid crystal, $F_i=\Delta\varepsilon' E^2/8\pi\cos^2\varphi_i$, depends on the dielectric anisotropy $\Delta\varepsilon'=\Delta\varepsilon\sin^2\theta$. In an antiferroelectric liquid crystal the term for the dielectric coupling ought to be considered for materials with low layer polarization and large pitch, when the distortion angle is nearly equal to π. In the pure dielectric regime the planar ferroelectric state [Fig. 2(e)] is not formed. In our paper we consider the polar mechanism of unwinding of the antiferroelectric helix.

Let us now examine the peculiarities of the phase transition to the synclinic state (Fig. 5). Without the barrier term in the free energy, this phase transition is of second order (squares in Fig. 5). Although the barrier term (3) does not change the energy of either the anticlinic or synclinic state, intermediate nonplanar states become less favorable in an electric field, and the transition to the homogeneous ferroelectric state ($\varphi_i^D=0$) is shifted to a lower field (Fig. 5, closed circles and diamonds). Another effect of the presence of the barrier term is a change of the phase transition type. Due to the biquadratic interaction, the F_b term is more important at low temperature, when the tilt angle is large. Even with the barrier term the transition at high temperature remains of second order (circles in Fig. 5), but becomes first order at low temperature (diamonds in Fig. 5). For the system presented in Fig. 5, the tricritical point at which the transition type changes from second to first order is at $T_C-T\approx8$ K. The transition to the synclinic state takes place in a field larger than the unwinding field ($E_s>2E_h$). This is the reason why the numerically calculated critical fields E_s agree well with fields obtained from analytical expressions without the chiral term [13]. At the first-order transition both the phase φ

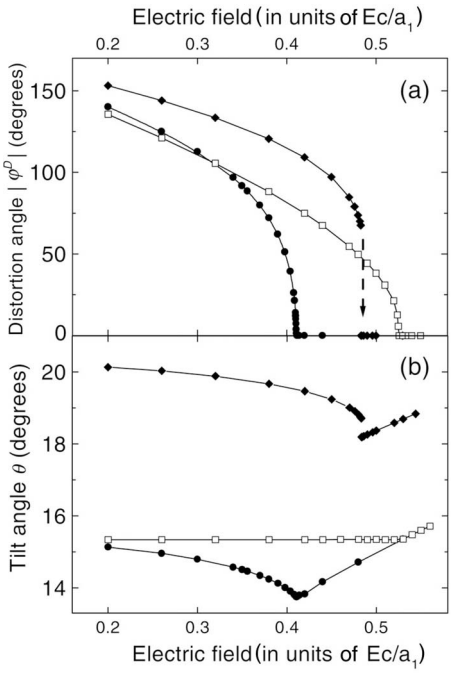

FIG. 5. Field dependence of the modulus of the distortion angle $|\varphi^D|$ (a) and the molecular tilt angle θ (b) in a distorted unwound antiferroelectric: The second-order transition without (squares) and with (circles) the barrier term. At the first-order transition both the phase and the modulus of the order parameter change discontinuously (diamonds). Distorted antiferroelectric with the barrier term shows a pronounced reverse electroclinic effect in which the tilt angle decreases with increasing field. Model parameters are $\alpha=0.01$, $a_1=5\times10^{-2}$, $f/a_1=4.2\times10^{-2}$, $a_2=0$, $T_C-T=7$ K without the barrier term and $\alpha=0.01$, $a_1=5\times10^{-2}$, $f/a_1=4.2\times10^{-2}$, $a_2=3\times10^{-2}$, $T_C-T=7$ K (second-order transition) and $T_C-T=12$ K (first-order transition) with the barrier term.

and the modulus θ of the order parameter change discontinuously [Figs. 5(a) and 5(b)].

In the distorted antiferroelectric state, θ decreases with increasing field [Fig. 5(b)]. This behavior is contrary to the well-known electroclinic effect in a ferroelectric structure when θ increases with field [8,27,34]. The "reverse" electroclinic effect was found in antiferroelectric liquid crystals with a barrier term for both the second- and first-order transitions (Fig. 5, circles and diamonds). Furthermore, the tilt angle also decreases at the first-order transition (Fig. 5, diamonds). This unusual behavior is replaced by the classical electroclinic effect, i.e., increase of the tilt angle with field after the transition to the synclinic state ($E>E_s$). However θ reaches its starting value (in the $E=0$ state) only at fields essentially higher than E_s (at $E>1.5E_s$ for the first-order transition). So, in a broad range of fields really used in experiments, the reverse electroclinic effect should be observed in antiferroelectric liquid crystals. Due to the anticlinic and barrier terms, synclinic ordering of the system in the electric field is prevented by decrease in the layer polarization (negative electroclinic effect). In the planar ferroelectric state ($E>E_s$) the electric term (4) dominates and the positive electroclinic effect is observed in both ferroelectric and antiferroelectric materials. In our paper, most of the results are given for the model parameters $f/a_1=0.042$ and $a_1=5\times10^{-2}$. However we have performed calculations for a wide range of parameters, e.g., different a_1 in the range $5\times10^{-2}-5\times10^{-4}$ for fixed f/a_1. The sequence of structures formed in the electric field remains the same. The magnitude of the electroclinic effect depends on the values of a_1 and a_2. Decrease of a_1 and a_2 leads to decrease of E_s and of the electroclinic effect. The behavior of an antiferroelectric phase in an electric field was previously considered by Parry-Jones and Elston [31]. They concentrated mostly on the unwinding regime. Their model did not consider a barrier term, structures with first-order phase transitions, or the electroclinic effect. However, the main features of the switching process to a nonhelical antiferroelectric and the sequence of states are consistent with our calculations.

In summary, we have calculated the structural transformations of an antiferroelectric liquid crystal in external electric field. The coupling of helicity and anticlinic ordering leads to formation of complex structures and cooperative motion of molecules. The antiferroelectric soliton can be removed only by the field-induced transition of the system to the synclinic state or by moving the soliton to the boundary of the sample. Full minimization of the free energy demonstrates coupling of the modulus and the phase of the order parameter. We found that the antiferroelectric shows an anomalous electroclinic effect in the electric field. The results of our calculations show that in an antiferroelectric phase a variety of unusual structures are realized in an electric field. For a detailed correlation of experimental phenomena with theory, further experimental and theoretical studies are required.

ACKNOWLEDGMENTS

This work was supported in part by the Russian Science Support Foundation, INTAS Grant No. 06-1000014-6462 and by Grant MK-2382.2007.2.

[1] P. G. de Gennes, Solid State Commun. **6**, 163 (1968).
[2] R. B. Meyer, Appl. Phys. Lett. **12**, 281 (1968).
[3] A. Michelson, L. Benguigui, and D. Cabib, Phys. Rev. A **16**, 394 (1977).
[4] H. Takezoe, K. Furuhata, T. Nakagiri, A. Fukuda, and E. Kure, Jpn. J. Appl. Phys. **17**, 1219 (1978).
[5] S. A. Pikin and V. L. Indenbom, Usp. Fiz. Nauk **125**, 251 (1978)[Sov. Phys. Usp. **21**, 487 (1978)].
[6] V. E. Dmitrienko andV. A. Beljakov, Zh. Eksp. Teor. Fiz. **78**, 1568 (1980)[Sov. Phys. JETP **51**, 787 (1980)].
[7] B. Kutnjak-Urbanc and B. Žekš, Phys. Rev. E **51**, 1569 (1995).
[8] N. Baytch, R. L. B. Selinger, J. V. Selinger, and R. Shashidhar, Phys. Rev. E **68**, 041702 (2003).

[9] F. Ghoddoussi, M. A. Pantea, P. H. Keyes, R. Naik, and P. P. Vaishnava, Phys. Rev. E **68**, 051706 (2003).
[10] Z. Kutnjak, Phys. Rev. E **70**, 061704 (2004).
[11] X. Y. Wang and P. L. Taylor, Phys. Rev. Lett. **76**, 640 (1996).
[12] X. Y. Wang, T. Kyu, A. M. Rudin, and P. L. Taylor, Phys. Rev. E **58**, 5919 (1998).
[13] T. Qian and P. L. Taylor, Phys. Rev. E **60**, 2978 (1999).
[14] A. Roy and N. V. Madhusudana, Eur. Phys. J. E **1**, 319 (2000).
[15] H. Sun, H. Orihara, and Y. Ishibashi, J. Phys. Soc. Jpn. **62**, 2706 (1993).
[16] M. Čepič and B. Žekš, Mol. Cryst. Liq. Cryst. Sci. Technol., Sect. A **263**, 61 (1995).
[17] B. Rovšek, M. Čepič, and B. Žekš, Phys. Rev. E **54**, R3113 (1996).
[18] B. Rovšek, M. Čepič, and B. Žekš, Phys. Rev. E **62**, 3758 (2000).
[19] D. Pociecha, E. Gorecka, M. Čepič, N. Vaupotič, B. Žekš, D. Kardas, and J. Mieczkowski, Phys. Rev. Lett. **86**, 3048 (2001).
[20] M. Čepič and B. Žekš, Phys. Rev. Lett. **87**, 085501 (2001).
[21] M. Čepič, D. Pociecha, B. Žekš, and H. T. Nguyen, J. Chem. Phys. **117**, 1817 (2002).
[22] P. V. Dolganov, V. M. Zhilin, V. E. Dmitrienko, and E. I. Kats, Pis'ma Zh. Eksp. Teor. Fiz. **76**, 579 (2002)[JETP Lett. **76**, 498 (2002)].
[23] P. V. Dolganov, V. M. Zhilin, V. K. Dolganov, and E. I. Kats, Phys. Rev. E **67**, 041716 (2003).
[24] D. A. Olson, X. F. Han, A. Cady, and C. C. Huang, Phys. Rev. E **66**, 021702 (2002).
[25] B. Rovšek, M. Čepič, and B. Žekš, Phys. Rev. E **70**, 041706 (2004).
[26] M. Conradi, I. Muševič, and M. Čepič, Phys. Rev. E **65**, 061705 (2002).
[27] P. G. de Gennes and J. Prost, *The Physics of Liquid Crystals*, 2nd ed. (Clarendon, Oxford, 1994).
[28] H. Orihara and Y. Ishibashi, Jpn. J. Appl. Phys., Part 2 **29**, L115 (1990).
[29] D. Pociecha, E. Gorecka, M. Čepič, N. Vaupotič, K. Gomola, and J. Mieczkowski, Phys. Rev. E **72**, 060701(R) (2005).
[30] E. Gorecka, A. Chandani, Y. Ouchi, H. Takezoe, and A. Fukuda, Jpn. J. Appl. Phys, Part 1 **29**, 131 (1990).
[31] L. A. Parry-Jones and S. J. Elston, Phys. Rev. E **63**, 050701(R) (2001).
[32] J.-K. Song, Atsuo Fukuda, and J. K. Vij, Phys. Rev. E **76**, 011708 (2007).
[33] J. P. F. Lagerwall, Phys. Rev. E **71**, 051703 (2005).
[34] S. Garoff and R. B. Meyer, Phys. Rev. Lett. **38**, 848 (1977).